Colloids and Surfaces B: Biointerfaces 151 (2017) 215–223

Contents lists available at ScienceDirect

Colloids and Surfaces B: Biointerfaces

journal homepage: www.elsevier.com/locate/colsurfb

Protocols

In vitro cytotoxicity evaluation of graphene oxide from the peroxidase-like activity perspective

Wei Zhang[a,1], Ying Sun[b,1], Zhichao Lou[a,c], Lina Song[a], Yang Wu[d], Ning Gu[a,*], Yu Zhang[a,*]

[a] State Key Laboratory of Bioelectronics, Jiangsu Key Laboratory for Biomaterials and Devices, School of Biological Science and Medical Engineering & Collaborative Innovation Center of Suzhou Nano Science and Technology, Southeast University, Nanjing 210096, PR China
[b] Patent Examination Cooperation Jiangsu Centre of the Patent Office, SIPO, Suzhou 215163, PR China
[c] College of Materials Science and Engineering, Nanjing Forestry University, Nanjing 210000, PR China
[d] Research Centre of Clinical Oncology, Jiangsu Cancer Hospital, Nanjing 210009, PR China

ARTICLE INFO

Article history:
Received 14 November 2015
Received in revised form
29 November 2016
Accepted 18 December 2016
Available online 19 December 2016

Keywords:
Graphene oxide
Hemin
Peroxidase mimics
Cytotoxicity
Reactive oxygen species

ABSTRACT

In this study, PEGylated graphene oxide (PEG-GO)-hemin composite structure was constructed. Hemin in the form of nanoscaled aggregates were immobilized on PEG-GO sheets by the π-π stacking supermolecular interaction. Via catalyzing the oxidation of chromogenic substrates, we elicited the obtained PEG-GO-Hemin composite sheets have much higher peroxidase-like activity compared to hemin or PEG-GO alone, which is due to the introduction of enzyme active center of hemin with high dispersity, the excellent affinity to organic substrate through π-π stacking and/or electrostatic adsorption and the rapid electron transfer capability of PEG-GO. Similarly, PEG-GO-Hemin was found to be able to catalyze the oxidation of low density lipoprotein (LDL) by H_2O_2, resulting in toxicity to porcine iliac endothelial cells (PIECs) in vitro. Furthermore, we also demonstrated that PEG-GO sheets showed enhanced peroxidase activity when met hemin containing proteins including hemoglobin and cytochrome c. High glucose level (HG) in human umbilical vein endothelial cells (HUVECs) can induce cytochrome c to release from the respiratory chain, thus applying PEG-GO under HG condition could cause a much higher peroxidase-like activity, resulting in the production of hydroxyl radical (•OH) and cytochrome c radical (cytochrome c•), which eventually enhance the apoptosis. These results suggest GO has potential hazard for biomedical applications in some pathophysiological conditions.

1. Introduction

Graphene, a very recent rising star with novel one-atom-thick two-dimensional (2D) graphitic carbon system, has recently emerged as a fascinating material [1–3]. The studies on graphene have attracted considerable attention from both the experimental and theoretical scientific communities [4–6]. In particular, the low cost and mass production of chemically exfoliated graphene oxide (GO) and reduced GO sheets possessing many reactive oxygen-containing groups for further functionalization and tuned properties has been realized [7–9]. The presence of oxygen-containing groups in GO render it strongly hydrophilic and water soluble, and also offer a wide range of possibilities to synthesize graphene-based functional materials for various applications, such as enhanced chemical catalysis, energy conversion and biomedical functions [10–14]. From the catalysis aspect, the peroxidase-like activity of PEGylated graphene oxide (PEG-GO) was weak due to the lack of enzyme active center, but the fact that PEG-GO displays rapid electron transferring and substrate adsorbing capacities in the catalytic reaction endows it great potential in catalytic activity enhancement, making PEG-GO a kind of new functional carrier material to construct organic molecules or nanoparticle-graphene composites. Hemin is a protoporphyrin with Fe^{3+} in a high spin state, and it is the stable oxidized form of heme which is the active catalytic center of natural enzyme such as horseradish peroxidase (HRP) and cytochromes [15,16]. In fact, hemin itself possesses intrinsic peroxidase activity which has been extensively investigated as an enzyme mimics [17]. Inspiring by the characteristics of GO and hemin, PEG-GO and hemin composite structure (PEG-GO-Hemin) with strong peroxidase-like activity was constructed in this paper. The hemin molecules were immobilized on the PEG-GO

* Corresponding authors.
E-mail addresses: guning@seu.edu.cn (N. Gu), zhangyu@seu.edu.cn (Y. Zhang).
[1] These authors contributed equally to this work.

http://dx.doi.org/10.1016/j.colsurfb.2016.12.025
0927-7765/

sheets by a simple wet-chemical strategy through π-π stacking interaction. The as obtained PEG-GO-Hemin exhibited much stronger peroxidase-like activity than hemin alone.

Many researches about GO's biocompatibility and its influence on bodily functions have been proposed [18–26]. The toxicity of GO was generally considered to be related to the interaction of cell membrane and GO [19,20,27], wrapping of cells by GO [21,22] and ROS generation [23,24,28,29]. Prime GO was believe to be toxic while the toxicity can be reduced via functionalizing with hydrophobic molecules including polyethylene glycol (PEG) [14,30], chitosan [31,32], artificial peroxidase [33], fetal bovine serum (FBS) [27] and polyethylenimine (PEI) [34]. In this paper, PEG-GO was chosen because its cytotoxicity is much lower than GO. Moreover, ROS level in cells treated with nanomaterials was closely related to the catalytic activity of the materials [35], hence ROS generation was the most important consideration in our study.

As reported, hemin, the most abundant form of human iron, can intercalate into native LDL and markedly catalyze LDL oxidation by a small amount of H_2O_2 [36]. Although native LDL is not toxic to endothelium, oxidized LDL (ox-LDL) can damage endothelium by denaturing cellular membranes and organelles and thus ox-LDL is one of the most important incentives of atherosclerosis [37–39]. The catalytic activity of hemin was significantly upgraded when combined with GO, implying possible toxicity of GO in vivo by enhanced catalytic oxidation. Here we demonstrated that the PEG-GO-Hemin provoked an enhanced catalytic oxidation of LDL, resulting consequently in an obvious toxicity for endothelial cells. From the peroxidase-like activity evaluation results, we found that in addition to hemin, the enhancement of peroxidase-like activity was also found when PEG-GO met hemin-containing proteins such as hemoglobin and cytochrome c. When exposed to hemin containing proteins such as leaked cytochrome c in human umbilical vein endothelial cells (HUVECs) incubated under high glucose level (HG), PEG-GO accelerated the cell apoptosis due to the elevated oxidation effect induced by hydroxyl radical (•OH) and cytochrome c radical (cytochrome c•) generated from the enhanced peroxidase-like activity. In general, although functionalization with PEG apparently reduced GO's toxicity, the PEG-GO may accelerate the apoptosis in cells under oxidative stress conditions, which is very likely attributed to the enhancement of oxidation effect. Our results indicate a potential hazard for in vivo biomedical application of GO-based composites under oxidative stress-induced pathological conditions such as atherosclerosis and diabetes.

2. Materials and methods

2.1. Materials

All chemicals used in the experiment were analytical grade reagent and were used as received. Polyethylene glycol (PEG) modified graphene oxide (PEG-GO) was provided by Nanjing Nanoeast Biotech Co. Ltd., which were synthesized from natural graphite by Hummers' Method and conjugated with amine-terminated six-armed PEG molecules via EDC chemistry [14,40,41]. Hemin (ferriprotoporphyrin chloride), 2,2′-azinobis (3-ethylbenzothiozoline)-6-sulfonic acid (ABTS), 3,3′,5,5′-tetramethylbenzidine (TMB), glucose oxidase (GOD), 30% H_2O_2, glucose, fructose, maltose, lactose, low density lipoprotein (LDL L-7914), lactoferrin (L-4040), ferritin (F-7879), transferrin (T3309), hemoglobin (H-2625) and cytochrome c (C-3438) were obtained from Sigma-Aldrich. PIEC and HUVEC were purchased from the Shanghai Cell Bank. Glacial acetic acid, anhydrous sodium acetate were purchased from Sinopharm Chemical Reagent Co. Ltd. Dipotassium hydrogen phosphate, sodium phosphate dibasic, sodium chloride, and tetramethyl ammonium hydroxide were reagents from Shanghai LingFeng Chemical Reagent Co. Ltd. Deionized water used throughout all experiments was purified with the Millipore system.

2.2. Synthesis of PEG-GO-Hemin composite sheets

PEG-GO-Hemin composite sheets were prepared as followed: PEG-GO was suspended in deionized water under ultrasonication (output power 180 W) for 10 min to obtain homogeneous single layered PEG-GO sheets. Meanwhile, hemin was suspended in deionized water (pH 7.8) under ultrasonication (output power 180 W) for 10 min to obtain homogeneous hemin solution. Then 20.0 mL of the homogeneous PEG-GO dispersion (7.5 μg/mL) was mixed with 20.0 mL of hemin aqueous solution (7.5 μg/mL), with a weight ratio of PEG-GO to hemin of 1:1, and the mixture was ultrasonicated for 30 min (output power 180 W). The dispersion was purified by an Ultrafiltration system for removing the excessive free hemin which was not immobilized on GO sheets. After that the PEG-GO-Hemin composite sheets were obtained and dispersed in water.

2.3. Characterization of PEG-GO-Hemin composite sheets

A JEOL JEM-2100 transmission electron microscope (TEM) was employed to observe the morphology of the PEG-GO-Hemin composite sheets and hemin. Agilent PicoPlus atomic force microscopy (AFM) was used to measure the thickness of the PEG-GO-Hemin composite sheets. Ultraviolet visible (UV-vis) absorption spectra were recorded on an UV–vis spectrophotometer (Shimadzu UV-3600, Japan). The peroxidase-like activity and the Michaelis constants were measured by a Bio-rad 680 microplate reader. An Optima 5300DV Inductive Coupled Plasma Emission Spectrometer (ICP) was used to detect the load rate of hemin on PEG-GO-Hemin composite sheets. A Brookhaven Zetaplus dynamic light scattering was used to measure the hydrodynamic size and zeta potential of PEG-GO-Hemin composite sheets. Infrared (IR) spectroscopy (NEXUS870) was used to characterize the structure of PEG-GO. Raman spectroscopy (JY HR800) using an Nd-YAG laser source operating at a wavelength of 532 nm was applied at room temperature. Pyris 1 thermal gravimetric analyzer was employed for investigating the rate process of reduction of PEG, GO and PEG-GO.

2.4. Peroxidase-like activity of PEG-GO-Hemin and kinetic analysis

The catalytic reaction was carried out in the NaAc-HAc buffer (0.2 M, pH 3.6) with 0.622 mM TMB (or 0.396 mM ABTS) and 852 mM hydrogen peroxidase as substrates, using PEG-GO-Hemin composite sheets as peroxidase-like mimic enzyme. The absorbance values at 650 nm for TMB oxidized product (or 405 nm for ABTS oxidized product) in the reaction system catalyzed by PEG-GO-Hemin composite sheets, PEG-GO, and hemin. Each at the same Fe concentration was recorded for 3 min with the microplate reader for comparing their activities.

Steady state kinetic assays were carried out using a microplate reader at room temperature. The reaction system was NaAc-HAc buffer (0.2 M, pH 3.6) in a 96-well plate containing H_2O_2 and TMB (or ABTS) as substrates and PEG-GO-Hemin composite sheets, PEG-GO or hemin as peroxidase-like enzyme. The kinetic assay of TMB (or ABTS) as the substrate was performed by adding 32 μL 30% H_2O_2 and different amounts (0.5, 1, 2, 4, 6, 8, 10 μL) of TMB solution (10 mg/mL, dissolved in DMSO) or ABTS solution (10 mg/mL, dissolved in deionized water). The kinetic assay of H_2O_2 as the substrate was performed by adding 10 μL TMB or ABTS and different amounts (0, 2, 4, 6, 8, 16, 32 μL) of 30% H_2O_2 solution. All the reactions were monitored in timescan mode at 650 nm for TMB or 405 nm for ABTS using the microplate reader.

Catalytic parameters were determined by fitting the absorbance data to the Michaelis–Menten equation [42] (1).

$$v = \frac{v_{max}[S]}{K_M + [S]} \quad (1)$$

The Michaelis–Menten equation describes the relationship between the rates of substrate conversion by the enzyme and the concentration of the substrate. In this equation, v is the rate of conversion, v_{max} is the maximum rate of conversion, [S] is the substrate concentration, and K_m is the Michaelis constant. The Michaelis constant is equivalent to the substrate concentration at which the rate of conversion is half of v_{max} and K_m approximates the affinity of the enzyme for the substrate.

2.5. Catalyzed oxidation of enzyme substrates by PEG-GO-Hemin upon H_2O_2 generation from GOD catalyzed glucose oxidation system

Glucose of different concentrations (0.001 μM-6.4 mM) was dissolved in 12 mM benzoic acid and stored for over 24 h before use. GOD was dissolved in phosphate buffer (pH 5.4) and kept in 4 °C refrigerator. PEG-GO-Hemin composite sheets (25 μg/mL) and GOD (0.58 mg/mL) were mixed together, followed by adjusting pH to 5.4 and stirring for 10 min to form a PEG-GO-Hemin-GOD hybrid. The catalytic reaction was carried out in the NaAc-HAc buffer (800 μL, pH 5.4) with TMB (50 μL, 10 mg/mL), PEG-GO-Hemin-GOD (50 μL) and glucose solution (100 μL) at different concentration. The as obtained mixture was incubated at 37 °C for 1 h, and then detected by monitoring the absorbance of TMB oxidation products at 650 nm on an UV–vis spectrophotometer (Shimadzu UV-3600, Japan). In control experiments, 32 mM maltose, 32 mM lactose, and 32 mM fructose were used instead of 16 mM glucose for investigating its selectivity.

2.6. ELISA detection of ox-LDL generated by PEG-GO-Hemin catalyzed oxidation of LDL in the presence of H_2O_2

We used Human oxidized low density lipoprotein, ox-LDL, ELISA Kit in order to verify whether ox-LDL was generated or not when using PEG-GO-Hemin or hemin to catalyze oxidation of LDL in the presence of H_2O_2. The Kit utilizes a competitive method to detect ox-LDL and thus in the Kit ox-LDL had been immobilized microtiter plate. Samples used in this experiment were different concentrations of LDL solution (150 or 300 μg/mL) with H_2O_2 (250 μM) catalyzed by PEG-GO-Hemin (28 μg/mL) or Hemin (18 μg/mL). The each sample was first added to the microtiter plate with three repeated wells and subsequently 50 μL HRP/anti-ox-LDL-antibody conjugate was added to each well. The mixtures were incubated for 1 h at 37 °C and then were washed with wash buffer for 5 times. After that, 90 μL HRP substrates (TMB and H_2O_2) were added to each well and incubated at 37 °C for 20 min under dark condition. Add 50 μL of stop solution to each well and finally determine the optical density within 5 min at 450 nm using a microplate reader. Three blank wells without adding any sample, three positives wells with ox-LDL standard sample, and three negative wells with LDL were also set as control groups. Blank: nothing; Positive: 5 μL standard diluent + 45 μL standard diluent. Negative: 10 μL LDL (300 μg/mL) + 40 μL standard diluent; Sample 1: 10 μL LDL (300 μg/mL) + 10 μL H_2O_2 (250 μM) + 10 μL PEG-GO-Hemin (28 μg/mL) + 20 μL standard diluent; Sample 2: 10 μL LDL (300 μg/mL) + 10 μL H_2O_2 (250 μM) + 10 μL PEG-GO-Hemin (18 μg/mL) + 20 μL standard diluent; Sample 3: 10 μL LDL (150 μg/mL) + 10 μL H_2O_2 (250 μM) + 10 μL PEG-GO-Hemin (28 μg/mL) + 20 μL standard diluent; Sample 4: 10 μL LDL (150 μg/mL) + 10 μL H_2O_2 (250 μM) + 10 μL PEG-GO-Hemin (18 μg/mL) + 20 μL standard diluent.

2.7. Peroxidase-like activity of PEG-GO mixed with all kinds of iron-containing proteins

Lactoferrin, ferritin, transferrin, hemoglobin and cytochrome c were chosen to research the effect of iron-containing proteins on the peroxidase-like activity of GO. The reaction system is as follows: 800 μL HAc-NaAc (pH 3.6) + 50 μL TMB + 10 μL catalyst (GO-proteins, GO or proteins alone) + 32 μL H_2O_2. After incubation at 20 °C for 3 min, absorption at 650 nm was detected using a microplate reader.

2.8. Cytotoxicity assays

PIECs and HUVECs were incubated in RPMI 1640 medium supplemented with 10% FBS, penicillin (100 units/mL), and streptomycin (100 μg/mL) in a humidified atmosphere with 5% CO_2 at 37 °C. MTT method [43] was conducted to assess the cytotoxicity of prepared treatments. Hemin or PEG-GO-Hemin catalyzes H_2O_2 to oxidize LDL into ox-LDL, whose specific cytotoxicity to PIECs was determined by MTT method. The prepared treatments were LDL, catalyst (Hemin or PEG-GO-Hemin) and H_2O_2 incubated for 6 h in advance. PIECs were seeded into 96-well plates (~1×10^4 cells/well) and incubated for 24 h beforehand. After removing the culture medium, 100 μL fresh medium containing 10 μL of the prepared treatments was added and then the cells were incubated continuously for different time. After 2–24 h incubation, 50 μL MTT was added into each well and the PIECs were subcultured for 4 h. After that, all liquid medium in each well was removed and 150 μL DMSO was added. A microplate reader (Model 680, Bio-rad, USA) was used to measure the optical density at 550 nm. MTT method was also used to evaluate the cytotoxicity of GO, PEG-GO, hemin, etc.

2.9. ROS detection

The oxidant-sensitivity dye DCFH-DA was used for ROS detection. HUVECs were plated in the 96-well plates (1×10^4 cells/well) and incubated for 24 h. GO samples were introduced to the cells with different concentrations and incubated for another 24 h or 48 h. The pre-treated cells were incubated with 10 μM DCFH-DA at 37 °C for 20 min in dark. The cells were then washed with PBS to remove the excess dye. Finally, the labeled cells were stored on ice, protected from light and taken photographs under fluorescence microscope (Zeiss) or collected DCF data using flow cytometry (FACS) or multimode reader (TECAN Infinite 200 PRO) with an excitation wavelength of 488 nm and an emission wavelength of 525 nm.

2.10. Cell apoptosis

Cell apoptosis and necrosis were analyzed by double staining with FITC-Annexin V and propidium iodide (PI) (KeyGen BioTECH, China), in which FITC-Annexin V binds to apoptotic cells with exposed phosphatidylserines (PS), while PI labelled necrotic cells with membrane damage. Cells in each 35 mm dish were collected and washed with PBS, the cells were resuspended with 500 μL binding buffer, next 5 μL FITC-Annexin V and 5 μL PI were added to the suspension and sorted with FCM. Data represent the mean fluorescence obtained from a population of 10,000 cells.

3. Results and discussion

3.1. Characterization of PEG-GO-Hemin composite sheets

IR spectroscopy (Fig. S1a) revealed the existence of C—O (~1100 cm^{-1}), C═O (~1600 cm^{-1}), C—H (~2900 cm^{-1}) and —OH

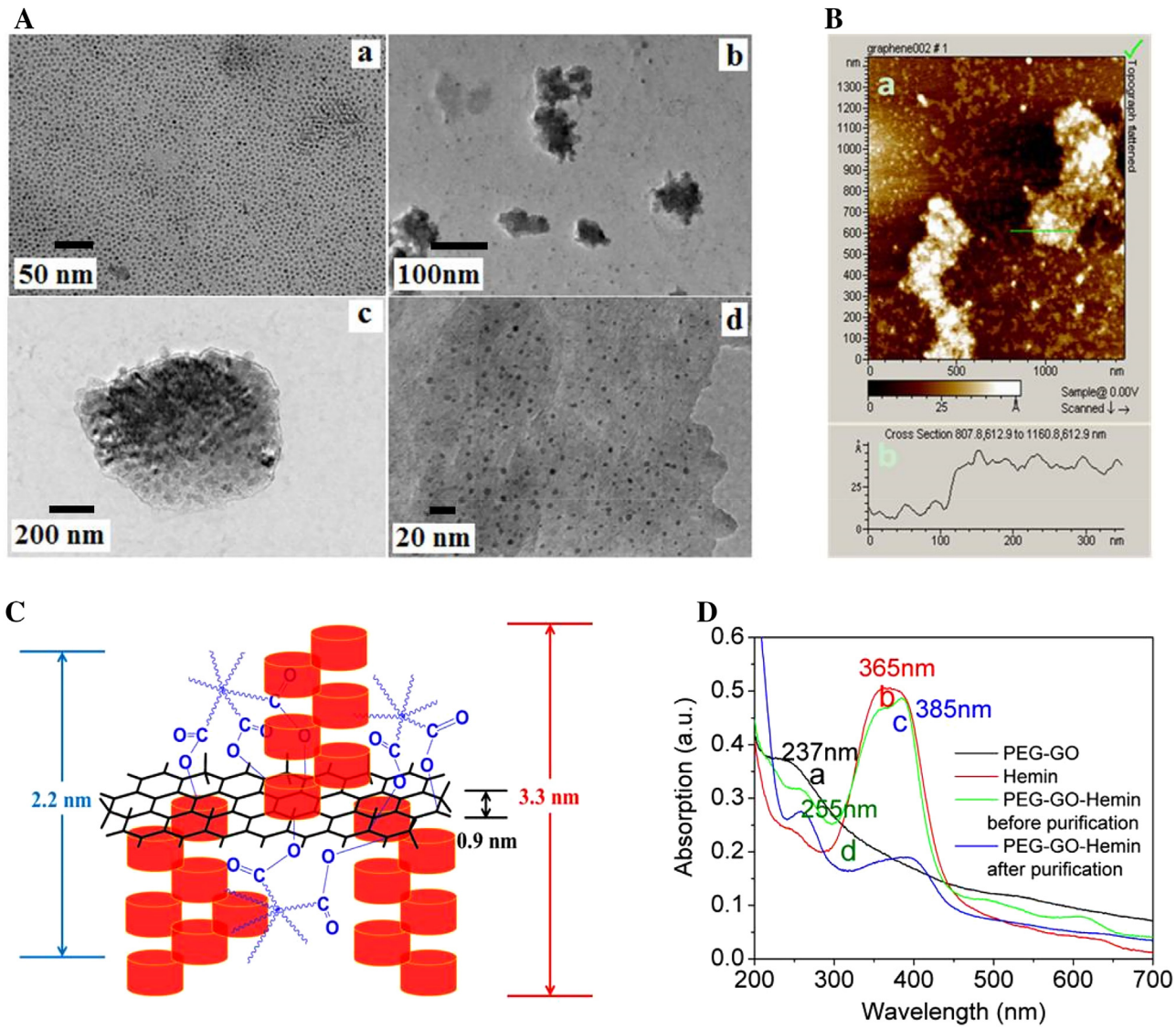

Fig. 1. Characterizations of PEG-GO-Hemin composite structure. (A) TEM images of hemin aggregates at pH 9 condition (a), hemin aggregates at pH 4 condition (b), GO-Hemin composite nanosheets (c) and the amplification (d) of a selected area in figure (c). (B) AFM image of GO-Hemin composite sheets and AFM profile measurement of green line marked position. (C) Calculation of layers of hemin molecules immobilized on PEG-GO sheets according to their thicknesses. (D) UV–vis absorption spectra of GO (a), hemin (b), GO-Hemin before (c) and after (d) purification. (For interpretation of the references to color in this figure legend, the reader is referred to the web version of this article.)

($\sim$3400 cm^{-1}) functional groups in PEG-GO. Thereinto, the C—H and C—O vibration bands confirmed the PEGylation of GO. TGA curves (Fig. S1b) indicate PEG-GO shows higher thermal stability than GO, according to the curves of GO-PEG and PEG, we can infer the mass percentage of PEG in PEG-GO sheets is approximately 70%. As shown in the Raman spectrum of PEG-GO (Fig. S1c), there is a G band (1600 cm^{-1}) originated from the phonon scattering of graphitic structure and a D band (1350 cm^{-1}) relating to graphite edges [44,45]. Fig. S1d gives the hydrodynamic size distribution of the obtained GO and PEG-GO sheets in water, showing two normal distributions in the size range of 150–400 nm and 400–1400 nm, consistent with the morphology characterized by TEM (Fig. 1A-c) and AFM (Figs. S1e and 1B). The thickness of PEG-GO was observed by AFM (Fig. S1e), the data revealed that most of the PEG-GO sheets topographic height of 2.2 nm with 0.66 nm PEG on both sides, thus the thickness of GO was about 0.9 nm, which is in accord with the typical single-layer exfoliated sheets prepared through Hummers' method [40].

Hemin was introduced as active center to construct PEG-GO-Hemin composite structure to mimic peroxidase. The mechanism for the hemin catalyzed reaction has been proposed and the intermediate states involved are believed to be similar to the intermediate states observed in the HRP-catalyzed reaction [17]. It will be a promising and cheap alternative to peroxidase mimics if their water dissolubility at low pH level was no longer a problem. In order to investigate the dispersive state of hemin in aqueous solution of different pH levels, hemin was dissolved in 0.1 M NaOH solution and then the pH of the solution was adjusted. TEM was used to observe the state of hemin, consequently indicating that hemin could be only dispersive at high pH levels (pH 8–12) as very small nanoscale aggregates (3–5 nm) as shown typically in Fig. 1A-a, however, visible hemin aggregates started to precipitate from the solution when the pH was lower than 7. Typically, larger granular aggregates can be clearly seen at pH 4 (Fig. 1A-b). TEM image of the obtained PEG-GO-Hemin dispersed in aqueous solution of pH 4 (Fig. 1A-c) and the partial amplification image (Fig. 1A-d) show that hemin was combined on PEG-GO in the form of very small nanoscaled aggregates. Noteworthy, the as obtained PEG-GO-Hemin could keep good dispersity in wide range of pH 2 $\sim$ 12, indicating that hemin loaded onto PEG-GO would avoid forming

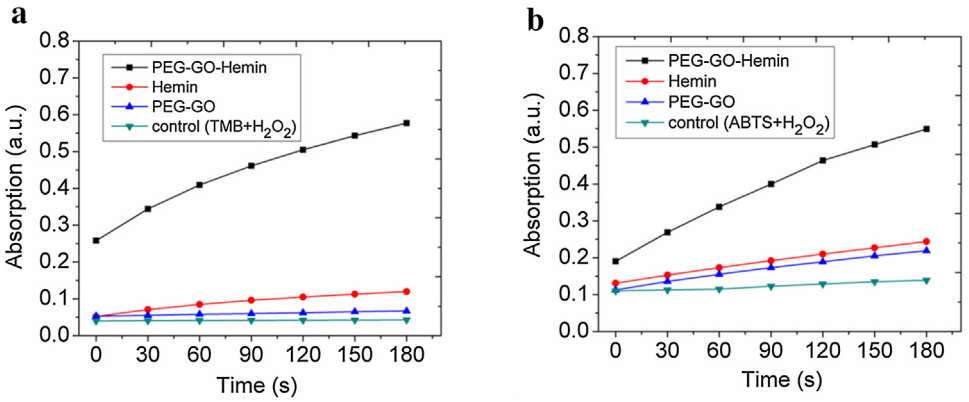

Fig. 2. The peroxidase-like activity of PEG-GO (15 μg/mL), hemin (10 μg/mL) and PEG-GO-Hemin composite sheets (25 μg/mL) measured respectively with TMB (a) and ABTS (b) as substrates in the presence of H_2O_2.

larger aggregates, insuring the exposure of more active Fe^{3+} centers [46]. Fig. 1B shows that the thickness of PEG-GO-Hemin was about 3.3 nm. The structure of PEG-GO-Hemin composite structure was shown in Fig. 1C. Since hemin could locate on both sides of the GO, the thickness of the hemin aggregates was roughly estimated to be about 1.2 nm. As reported in literatures [47], the hemin molecule can be considered as a cylinder with 0.2 nm thickness and 1.2 nm long, thus it is deduced that hemin aggregates are composed of about 6 layers of hemin molecules. In addition, ICP-OES measurement was used to detect the iron content of pure PEG-GO-Hemin composite sheets to calculate the load rate of hemin, which is calculated to be approximately 40% by weight. Zeta potential measurement indicated the PEG-GO-Hemin has a charge of −32 mV, originating from the negatively charged carboxyl groups in hemin and PEG-GO. Fig. 1D shows UV–vis absorption spectra of hemin, PEG-GO, PEG-GO-Hemin before and after purification. It can be seen that the characteristic peak of PEG-GO appeared at ~237 nm (Fig. 1D-a), which moved to 255 nm (Fig. 1D-c, d) when PEG-GO sheets were covered by hemin aggregates [14,46,48,49]. Upon the combination with PEG-GO, the intense Soret band (B-band) of the hemin aggregates (at ~365 nm) became split and red-shifted to ~385 nm (Fig. 1D-b, c) [50–53]. After purification, the free hemin aggregates were removed (Fig. 1D-c, d), pure PEG-GO-Hemin composite sheets were obtained with typical PEG-GO and hemin absorption peaks at 255 nm and 385 nm respectively.

3.2. Peroxidase-like activity of PEG-GO-Hemin composite sheets

It is known that hemin is the active site of peroxidase and exhibits the peroxidase-like activity [17]. So PEG-GO-Hemin composite sheets are expected to display peroxidase-like activity. As illustrated in Fig. 2, the peroxidase-like activity was monitored through a colorimetric reaction using chromogenic substrates TMB/ABTS in the presence of H_2O_2. It can be seen that the PEG-GO-Hemin composite sheets have a much higher catalytic activity than hemin or PEG-GO alone, suggesting that the effective combination of hemin and PEG-GO, the latter played an important role in the enhancement of peroxidase-like activity. More specially, PEG-GO served as a functional carrier support to largely enhance the activity of catalytic center of hemin, due to its rapid electron transfer ability and high substrate adsorption capacity [54]. Furthermore, Fig. S2 shows that the pH and temperature dependences of peroxidase-like activities of hemin and PEG-GO-Hemin have the similar trend, with the optimum reaction conditions of pH 3.6 and 55 °C.

3.3. Steady state enzyme kinetics

The peroxidase-like activity of the PEG-GO-Hemin composite sheets was also investigated by determining the apparent steady-state kinetic parameters of the catalytic reaction. With the suitable range of TMB or ABTS concentrations, typical Michaelis-Menten curves were observed for hemin aggregates (data not shown), PEG-GO (data not shown), and PEG-GO-Hemin composite sheets (Fig. S3). The Michaelis constant (K_m) and the maximal reaction velocity (v_{max}) data were obtained by fitting the experimental data to the Michaelis-Menten model (Table 1). The apparent K_m values of the PEG-GO with both TMB and ABTS as substrates were lower than those of hemin alone, suggesting that the PEG-GO has a higher affinity to the substrates than hemin. This can be readily understood by considering the aromatic ring structure of the substrate of TMB or ABTS, which leads to a stronger π-π stacking interaction with PEG-GO than hemin. The apparent K_m value of PEG-GO-Hemin composite sheets with TMB as substrate was significantly lower than that of ABTS, suggesting that the PEG-GO-Hemin composite sheets had higher affinity to TMB than ABTS. This may be mainly attributed to strong electrostatic adsorption between the negatively charged PEG-GO-Hemin composite sheets and the positively charged TMB. The apparent K_m value of PEG-GO-Hemin composite sheets with TMB or ABTS as substrate was larger than that of PEG-GO and hemin, suggesting PEG-GO-Hemin composite sheets had lower affinity for the substrates than PEG-GO and hemin. However, the apparent v_{max} value of PEG-GO-Hemin composite structure was much higher than any of PEG-GO and hemin, according with the results shown in Table 1. Both of the PEG-GO and hemin had

Table 1
Comparison of the kinetic parameters of PEG-GO, hemin and PEG-GO-Hemin composite sheets. K_m is the Michaelis constant and v_{max} is the maximal reaction velocity.

Catalyst	Substrate	K_m (mM)	v_{max} (Ms^{-1})
PEG-GO	TMB	0.032	3.00×10^{-7}
PEG-GO	ABTS	0.035	1.92×10^{-6}
Hemin	TMB	0.394	8.69×10^{-6}
Hemin	ABTS	0.135	6.23×10^{-6}
PEG-GO-Hemin	TMB	1.067	3.47×10^{-5}
PEG-GO-Hemin	ABTS	1.567	5.43×10^{-5}

aromatic conjugation structures, a π-π interaction could be considered as a dominant role to facilitate the substrate adsorption and enrichment around the catalytic centers of hemin assembled on PEG-GO sheets. The substrate enrichment may result in the high peroxidase-like activity of the PEG-GO-Hemin composite sheets. On the other hand, compared with hemin in the reaction buffer of pH 3.6, the enhanced exposure of active centers of hemin when loaded on GO also contributed to the high peroxidase-like activity of the PEG-GO-Hemin composite sheets. Similarly, GO-enhanced catalytic activity has been found in GO-TiO_2, GO-Fe_3O_4 and GO-Pt systems [55–59].

According to the literature [60], natural HRP possesses K_m values of 0.434 mM and 3.70 mM with TMB and H_2O_2 as substrates respectively. In contrast, the K_m value (0.18 mM) of the PEG-GO-Hemin composite sheets with H_2O_2 as substrate is much lower than HRP, suggesting that the hybrids have a higher affinity for H_2O_2 than HRP. However, the affinity to TMB (K_m = 1.067 mM) does not improve for the PEG-GO-Hemin composite sheets compared to HRP. The small K_m values for H_2O_2 mean that a lower concentration of H_2O_2 is required to reach the v_{max} for PEG-GO-Hemin composite sheets, as shown in Fig. S3c and d.

3.4. Substrate oxidation capability of PEG-GO-Hemin upon H_2O_2 generation from GOD catalyzed glucose oxidation system

It was known that glucose and oxygen can be catalyzed by the GOD to produce the gluconic acid and H_2O_2, thus a GOD-glucose system was chosen to verify the strong peroxidase-like activity of PEG-GO-Hemin composite structure [61,62]. Upon H_2O_2 generation from this simulative biological system, PEG-GO-Hemin composite sheets can catalyze the oxidation of peroxidase substrates like TMB. As shown in Fig. S4a, GOD catalyzed the production of H_2O_2, who then oxidize TMB to form a blue colored product (oxidized TMB) under the catalysis of PEG-GO-Hemin composite sheets. Fig. S4b and c show that using PEG-GO-Hemin-GOD complex enzyme system, glucose can be detected as low as 0.01 μM, and the linear range is from 0.1 μM to 25 μM. The detection of glucose at μM level means the formation of H_2O_2 at μM level, so that we can clearly see that with the help of PEG-GO-Hemin composite sheets, H_2O_2 even at μM level could be used to oxidize TMB. As shown in Fig. S5, the addition of PEG-GO leaded to an obvious enhancement of H_2O_2 generation in the GOD-glucose system, hence the high sensitivity was not only due to the high peroxidase-like activity of PEG-GO-Hemin and its strong affinity to H_2O_2 as demonstrated above, but also the influence of PEG-GO on catalytic activity of GOD ($p < 0.05$). Moreover, the data showed PEG-GO itself can enhance the oxidation of glucose ($p < 0.05$). Maltose, fructose and lactose were also chosen to evaluate the specificity of H_2O_2 generation from the PEG-GO-Hemin-GOD system. As shown in Fig. S6, even the concentrations of maltose, fructose and lactose were as high as 32 mM, the signal remained as low as the background signal. This specificity is due to the high affinity and selectivity of GOD for glucose.

3.5. Cytotoxicity of PEG-GO-Hemin composite sheets from the peroxidase-like activity perspective

It is reported [36] that hemin-catalyzed LDL system can lead to cytotoxicity to endothelial cell in the presence of H_2O_2. Here a human ox-LDL ELISA Kit was used to detect whether there exists

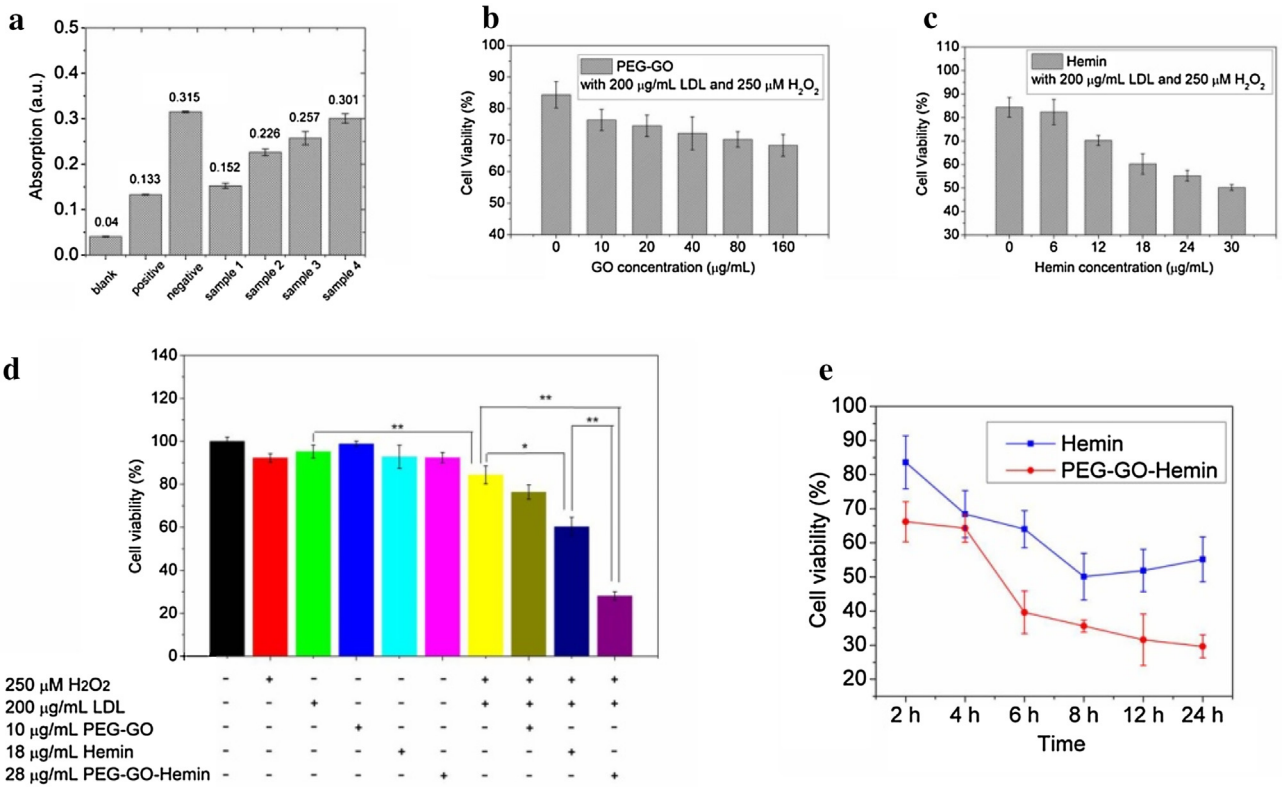

Fig. 3. (a) Human oxidized low density lipoprotein, ox-LDL ELISA Kit's results of different samples. Negative control: 60 μg/mL LDL; sample 1: 60 μg/mL LDL + 50 μM H_2O_2 + 5.6 μg/mL PEG-GO-Hemin; sample 2: 60 μg/mL LDL + 50 μM H_2O_2 + 3.6 μg/mL PEG-GO-Hemin; sample 3: 30 μg/mL LDL + 50 μM H_2O_2 + 5.6 μg/mL PEG-GO-Hemin; sample 4: 30 μg/mL LDL + 50 μM H_2O_2 + 3.6 μg/mL PEG-GO-Hemin. (b) Cell viability of PIECs treated with PEG-GO of different concentrations together with 200 μg/mL LDL and 250 μM H_2O_2. (c) Cell viability of PIECs treated with hemin of different concentrations together with 200 μg/mL LDL and 250 μM H_2O_2. (d) Cell viability of PIECs with different treatments. * and ** indicate $p < 0.05$ and $p < 0.01$, respectively, Student's *t*-test. (e) Specific toxicity to PIECs after 24 h of incubation with PEG-GO, Hemin and PEG-GO-hemin of different concentrations in the presence of LDL and H_2O_2.

ox-LDL in our prepared samples. This assay is on the base of the competitive inhibition between the pre-coated ox-LDL and ox-LDL generated in the samples. The experimental and control samples were added to the appropriate microtiter plate wells followed by labeling with HRP/anti-ox-LDL-antibody conjugate for detection of ox-LDL. A substrate solution was then added to the wells and the color develops in opposite to the amount of ox-LDL in each sample. Since this assay has high sensitivity and excellent specificity for the detection of ox-LDL, there is no significant cross-reactivity or interference between human ox-LDL and analogues. Fig. 3a shows the existence of ox-LDL in the experimental samples (sample 1, 2, 3 and 4) because the absorption values of the experimental samples were all between the optical density values of the positive and negative control. The absorption values of sample 1 and 3 are lower than sample 2 and 4, respectively, indicating more ox-LDL was induced by PEG-GO-Hemin of higher concentration. Meanwhile, higher LDL concentration means more ox-LDL could be generated in the oxidation process. In order to exclude included materials' cytotoxicity, we took each material as treatment for cytotoxicity tests. We studied the toxicity to PIECs caused by H_2O_2, LDL together with PEG-GO, hemin or PEG-GO-Hemin. According to the pre-test results (data not shown), we used 250 μM H_2O_2 and 200 μg/mL LDL to carry out the following experiments. As shown in Fig. 3b and c, PEG-GO and hemin can both potentiate the cytotoxicity of H_2O_2 and LDL in a concentration-dependent manner. To simplify the study, we chose PEG-GO-Hemin composite sheets without purification to carry out the subsequent research. 28 μg/mL PEG-GO-Hemin composite sheets without purification (or 18 μg/mL hemin), 250 μM H_2O_2 and 200 μg/mL LDL induced obvious cytotoxicity (Fig. 3d). Specifically, individual treatments with 250 μM H_2O_2, 200 μg/mL LDL, 10 μg/mL PEG-GO, 18 μg/mL hemin or 28 μg/mL PEG-GO-Hemin have little toxicity (cell viability >90%) to PIECs. Known from the yellow column in Fig. 3d, LDL and H_2O_2 together caused obvious cytotoxicity ($p < 0.01$), which may root in the toxicity of ox-LDL. Adding PEG-GO-Hemin or hemin in the culture medium containing LDL and H_2O_2 obviously increased the cytotoxicity ($p < 0.05$ for hemin, $p < 0.01$ for PEG-GO-Hemin), however, PEG-GO do not enhance the cytotoxicity of LDL with H_2O_2 ($p > 0.05$).Time course studies in Fig. 3e show specific toxicity to PIECs used here after 2–24 h of incubation with LDL, PEG-GO-Hemin (or hemin) and H_2O_2. After 24 h of incubation, the cell viability dropped down to approximately 29% and 55% for PEG-GO-Hemin and hemin respectively. Finally we make sure that PEG-GO-Hemin can catalyze H_2O_2 to oxidize LDL and eventually result in the cytotoxicity.

3.6. *Cytotoxicity of PEG-GO from the peroxidase-like activity perspective*

Many researches have reported the toxicity of nanoparticles may associate with the oxidative stress induced by them [49,63–67]. For example, Fe_3O_4 and Fe_2O_3 nanoparticles can induce oxidative stress and apoptosis to cultured human umbilical endothelial cells mainly because of the generation of ROS. In light of their peroxidase-like activity which could induce the generation of H_2O_2, we have to think about the introduction of GO or its derivatives to the human body still needs carefully. Fig. S7a shows that cytotoxicity of GO reduced when functionalized with PEG. Moreover, concentration of ROS in HUVECs and PIECs treated with GO obviously increased as GO concentration increased, however, ROS level in cells treated with PEG-GO increased a little (Fig. S7b). Furthermore, PEG-GO-Hemin showed higher cytotoxicity, which may induced by the increase of intracellular ROS level (Fig. S7c). As here-

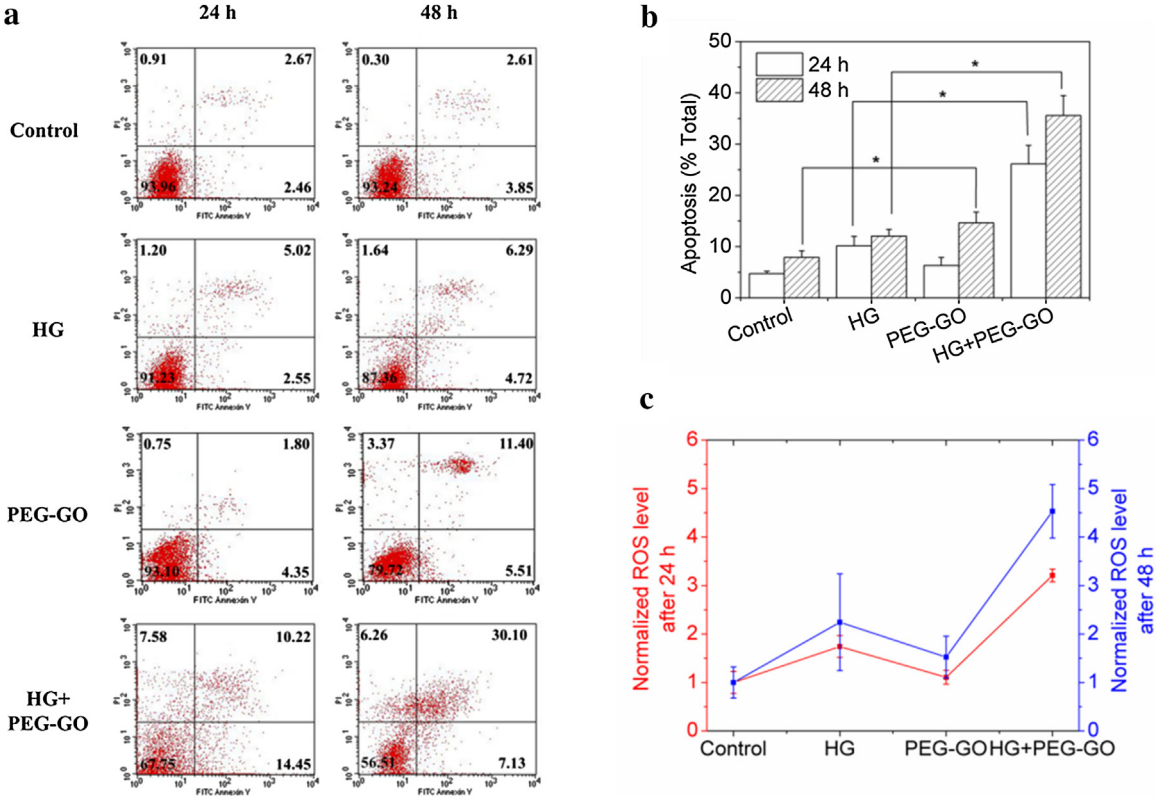

Fig. 4. The influence of GO on the aoptosis of HUVECs in the presence of HG. (A) HUVECs treated with HG (35 mM) alone, PEG-GO (100 μg/mL) alone or PEG-GO (100 μg/mL) and HG (35 mM) combined for apoptosis analysis, FACS results of the Annexin V-FITC and PI assay. (B) The summary of the apoptosis rate of HUVECs after exposed to HG (35 mM) alone, PEG-GO (100 μg/mL) alone or PEG-GO (100 μg/mL) and HG (35 mM) combined for 24 h and 48 h. The total apoptotic proportion includes the percentage of cells with fluorescence Annexin V+/PI- and Annexin V+/PI+. Data are mean ± SD of four independent experiments, * indicates $p < 0.05$, Student's *t*-test. (c) ROS level in HUVECs after exposure to PEG-GO of different concentrations for 24 h and 48 h. Data are mean ± SD of four independent experiments.

inbefore described, PEG-GO may be more toxic when combined with hemin, here we also considered about other common hemin-containing proteins in vivo. As shown in Fig. S8, when combining PEG-GO with hemin-containing proteins such as hemoglobin and cytochrome c, the catalytic ability of these proteins was significantly enhanced. Hence we inferred the nontoxic PEG-GO may be toxic when contact with hemin-containing proteins due to the enhanced peroxidase-like activity.

As a result of glucose auto-oxidation, metabolism and formation of advanced glycosylation end products, culturing cells with high glucose level (HG) will induce ROS generation [68,69], which is probably the upstream regulator of apoptosis. Moreover, the loss of mitochondria membrane potential and the apoptotic chromatin condensation in the nucleus were observed as the early signs of apoptosis, hence cytochrome c release takes place under HG condition [70,71]. Fig. S9 shows PEG-GO will induce apoptosis under HG condition owing to the generation of •OH and cytochrome c radicals (cytochrome c•). As shown in Fig. 4, when the cells were treated with HG (35 mM) or PEG-GO (100 μg/mL) alone for 24 h and 48 h, the apoptosic cells constituted $10.15 \pm 1.86\%$, $6.32 \pm 1.56\%$, $12.06 \pm 1.31\%$ and $14.62 \pm 2.12\%$, respctively. Where as they constituted $32.88 \pm 2.56\%$ and $35.59 \pm 3.88\%$ when HUVECs were treated with HG (35 mM) combined with PEG-GO (100 μg/mL). Although treating with 100 μg/mL PEG-GO alone for 24 h did not induce apoptosis, it is obvious the PEG-GO is able to augment the potency of HG induced cell apoptosis ($p < 0.01$). However, when incubated for 48 h, 100 μg/mL PEG-GO alone can induce obvious apoptosis of HUVECs ($p < 0.01$), which is resulted from mainly to the oxidative stress induced by PEG-GO [72]. As shown in Fig. 4c, when incubated 100 μg/mL PEG-GO for 48 h, overproduction of ROS occurs ($p < 0.05$ as compared to 24 h condition). Under normal circumstances, cytochrome c locate in the mitochondrial membrane, PEG-GO cannot contact with them, while in HG condition, cytochrome c release into the cytosol and even extracellular fluid, then PEG-GO can accelerate the electron transfer between cytochrome c and H_2O_2, which catalyze the more toxic •OH and cytochrome c• production [8,73].

4. Conclusions

In summary, the PEG-GO-Hemin composite sheets were successfully obtained by a simple π-π stacking super-molecular method. The existence of PEG-GO carrier makes hemin more stable as small nanoparticles in solutions of a wide range of pH levels. Furthermore, the obtained PEG-GO-Hemin composites have a much higher catalytic activity as peroxidase than hemin or PEG-GO alone. PEG-GO-Hemin composite sheets could oxidize chromogenic substrate TMB by using H_2O_2 even at μM level. In this report, we found that PEG-GO could enhance the oxidation of LDL to form ox-LDL, leading thus to PIECs' toxicity. It was also found that PEG-GO is able to augment the potency of HG induced cell apoptosis. We believe that PEG-GO-Hemin will show a broad application potential in biotechnology and medical diagnostics in vitro based on its peroxidase-like activity. Simultaneously, applications of PEG-GO or PEG-GO-Hemin in vivo still require carefully consideration since their toxicity to endothelial cells.

Conflict of interest

The authors declare no competing financial interest.

Acknowledgements

This research was supported by the National Important Science Research Program of China (Nos. 2011CB933503, 2013CB733800), National Natural Science Foundation of China (Nos. 81571806, 61601227, 81301870), the Basic Research Program of Jiangsu Province (Natural Science Foundation, Nos. BK2011036, BK20160939), Research Fund for the Doctoral Program of Higher Education of China (20110092110029).

Appendix A. Supplementary data

Supplementary data associated with this article can be found, in the online version, at http://dx.doi.org/10.1016/j.colsurfb.2016.12.025.

References

[1] C.e.N.e.R. Rao, A.e.K. Sood, K.e.S. Subrahmanyam, A. Govindaraj, Graphene: the new two-dimensional nanomaterial, Angew. Chem. Int. Ed. 48 (2009) 7752–7777.
[2] Y. Xu, H. Bai, G. Lu, C. Li, G. Shi, Flexible graphene films via the filtration of water-soluble noncovalent functionalized graphene sheets, J. Am. Chem. Soc. 130 (2008) 5856–5857.
[3] X.-W. Liu, Z.-J. Yao, Y.-F. Wang, X.-W. Wei, Graphene oxide sheet-prussian blue nanocomposites: green synthesis and their extraordinary electrochemical properties, Colloids Surf. B: Biointerfaces 81 (2010) 508–512.
[4] K.S. Novoselov, A.K. Geim, S. Morozov, D. Jiang, Y. Zhang, S. Dubonos, I. Grigorieva, A. Firsov, Electric field effect in atomically thin carbon films, Science 306 (2004) 666–669.
[5] C. Berger, Z. Song, X. Li, X. Wu, N. Brown, C. Naud, D. Mayou, T. Li, J. Hass, A.N. Marchenkov, Electronic confinement and coherence in patterned epitaxial graphene, Science 312 (2006) 1191–1196.
[6] I. Meric, M.Y. Han, A.F. Young, B. Ozyilmaz, P. Kim, K.L. Shepard, Current saturation in zero-bandgap, top-gated graphene field-effect transistors, Nat. Nanotechnol. 3 (2008) 654–659.
[7] J. Kim, F. Kim, J. Huang, Seeing graphene-based sheets, Mater. Today 13 (2010) 28–38.
[8] S. Stankovich, D.A. Dikin, R.D. Piner, K.A. Kohlhaas, A. Kleinhammes, Y. Jia, Y. Wu, S.T. Nguyen, R.S. Ruoff, Synthesis of graphene-based nanosheets via chemical reduction of exfoliated graphite oxide, Carbon 45 (2007) 1558–1565.
[9] A.B. Bourlinos, D. Gournis, D. Petridis, T. Szabó, A. Szeri, I. Dékány, Graphite oxide: chemical reduction to graphite and surface modification with primary aliphatic amines and amino acids, Langmuir 19 (2003) 6050–6055.
[10] B. Li, X. Cao, H.G. Ong, J.W. Cheah, X. Zhou, Z. Yin, H. Li, J. Wang, F. Boey, W. Huang, All-carbon electronic devices fabricated by directly grown single-walled carbon nanotubes on reduced graphene oxide electrodes, Adv. Mater. 22 (2010) 3058–3061.
[11] P.V. Kamat, Graphene-based nanoassemblies for energy conversion, J. Phys. Chem Lett. 2 (2011) 242–251.
[12] K. Yang, J. Wan, S. Zhang, Y. Zhang, S.-T. Lee, Z. Liu, In vivo pharmacokinetics, long-term biodistribution, and toxicology of PEGylated graphene in mice, ACS Nano 5 (2010) 516–522.
[13] X. Zhang, J. Yin, C. Peng, W. Hu, Z. Zhu, W. Li, C. Fan, Q. Huang, Distribution and biocompatibility studies of graphene oxide in mice after intravenous administration, Carbon 49 (2011) 986–995.
[14] Z. Liu, J.T. Robinson, X. Sun, H. Dai, PEGylated nanographene oxide for delivery of water-insoluble cancer drugs, J. Am. Chem. Soc. 130 (2008) 10876–10877.
[15] G. Zhang, P.K. Dasgupta, Hematin as a peroxidase substitute in hydrogen peroxide determinations, Anal. Chem. 64 (1992) 517–522.
[16] J.A. Akkara, J. Wang, D.-P. Yang, K.E. Gonsalves, Hematin-catalyzed polymerization of phenol compounds, Macromolecules 33 (2000) 2377–2382.
[17] S. Nagarajan, R. Nagarajan, R. Tyagi, J. Kumar, F.F. Bruno, L.A. Samuelson, Biocatalytic modification of naturally occurring iron porphyrin, J. Macromol. Sci. A 45 (2008) 951–956.
[18] O. Akhavan, E. Ghaderi, E. Hashemi, E. Akbari, Dose-dependent effects of nanoscale graphene oxide on reproduction capability of mammals, Carbon 95 (2015) 309–317.
[19] K. Wang, J. Ruan, H. Song, J. Zhang, Y. Wo, S. Guo, D. Cui, Biocompatibility of graphene oxide, Nanoscale Res. Lett. 6 (2011) 1.
[20] O. Akhavan, E. Ghaderi, Toxicity of graphene and graphene oxide nanowalls against bacteria, ACS Nano 4 (2010) 5731–5736.
[21] E. Hashemi, O. Akhavan, M. Shamsara, R. Rahighi, A. Esfandiar, A.R. Tayefeh, Cyto and genotoxicities of graphene oxide and reduced graphene oxide sheets on spermatozoa, RSC Adv. 4 (2014) 27213–27223.
[22] O. Akhavan, E. Ghaderi, A. Esfandiar, Wrapping bacteria by graphene nanosheets for isolation from environment, reactivation by sonication, and inactivation by near-infrared irradiation, J. Phys. Chem. B 115 (2011) 6279–6288.
[23] O. Akhavan, E. Ghaderi, A. Akhavan, Size-dependent genotoxicity of graphene nanoplatelets in human stem cells, Biomaterials 33 (2012) 8017–8025.
[24] Y. Zhang, S.F. Ali, E. Dervishi, Y. Xu, Z. Li, D. Casciano, A.S. Biris, Cytotoxicity effects of graphene and single-wall carbon nanotubes in neural phaeochromocytoma-derived PC12 cells, ACS Nano 4 (2010) 3181–3186.
[25] A.M. Pinto, I.C. Gonçalves, F.D. Magalhães, Graphene-based materials biocompatibility: a review, Colloids Surf. B: Biointerfaces 111 (2013) 188–202.

[26] H. Yue, W. Wei, Z. Yue, B. Wang, N. Luo, Y. Gao, D. Ma, G. Ma, Z. Su, The role of the lateral dimension of graphene oxide in the regulation of cellular responses, Biomaterials 33 (2012) 4013–4021.
[27] W. Hu, C. Peng, M. Lv, X. Li, Y. Zhang, N. Chen, C. Fan, Q. Huang, Protein corona-mediated mitigation of cytotoxicity of graphene oxide, ACS Nano 5 (2011) 3693–3700.
[28] Y. Li, Y. Liu, Y. Fu, T. Wei, L. Le Guyader, G. Gao, R.-S. Liu, Y.-Z. Chang, C. Chen, The triggering of apoptosis in macrophages by pristine graphene through the MAPK and TGF-beta signaling pathways, Biomaterials 33 (2012) 402–411.
[29] M.C. Duch, G.S. Budinger, Y.T. Liang, S. Soberanes, D. Urich, S.E. Chiarella, L.A. Campochiaro, A. Gonzalez, N.S. Chandel, M.C. Hersam, Minimizing oxidation and stable nanoscale dispersion improves the biocompatibility of graphene in the lung, Nano Lett. 11 (2011) 5201–5207.
[30] X. Sun, Z. Liu, K. Welsher, J.T. Robinson, A. Goodwin, S. Zaric, H. Dai, Nano-graphene oxide for cellular imaging and drug delivery, Nano Res. 1 (2008) 203–212.
[31] K.-H. Liao, Y.-S. Lin, C.W. Macosko, C.L. Haynes, Cytotoxicity of graphene oxide and graphene in human erythrocytes and skin fibroblasts, ACS Appl. Mater. Interfaces 3 (2011) 2607–2615.
[32] H. Fan, L. Wang, K. Zhao, N. Li, Z. Shi, Z. Ge, Z. Jin, Fabrication, mechanical properties, and biocompatibility of graphene-reinforced chitosan composites, Biomacromolecules 11 (2010) 2345–2351.
[33] C.X. Guo, X.T. Zheng, Z.S. Lu, X.W. Lou, C.M. Li, Biointerface by cell growth on layered graphene-artificial peroxidase-protein nanostructure for in situ quantitative molecular detection, Adv. Mater. 22 (2010) 5164–5167.
[34] L. Feng, S. Zhang, Z. Liu, Graphene based gene transfection, Nanoscale 3 (2011) 1252–1257.
[35] W. Zhang, S. Hu, J.-J. Yin, W. He, W. Lu, M. Ma, N. Gu, Y. Zhang, Prussian blue nanoparticles as multienzyme mimetics and reactive oxygen species scavengers, J. Am. Chem. Soc. 138 (2016) 5860–5865.
[36] M.B. Juckett, J. Balla, G. Balla, J. Jessurun, H.S. Jacob, G.M. Vercellotti, Ferritin protects endothelial cells from oxidized low density lipoprotein in vitro, Am. J. Pathol. 147 (1995) 782–788.
[37] K. Öörni, M.O. Pentikäinen, M. Ala-Korpela, P.T. Kovanen, Aggregation, fusion, and vesicle formation of modified low density lipoprotein particles: molecular mechanisms and effects on matrix interactions, J. Lipid Res. 41 (2000) 1703–1714.
[38] T. Sawamura, N. Kume, T. Aoyama, H. Moriwaki, H. Hoshikawa, Y. Aiba, T. Tanaka, S. Miwa, Y. Katsura, T. Kita, An endothelial receptor for oxidized low-density lipoprotein, Nature 386 (1997) 73–76.
[39] H. Morawietz, U. Rueckschloss, B. Niemann, N. Duerrschmidt, J. Galle, K. Hakim, H.-R. Zerkowski, T. Sawamura, J. Holtz, Angiotensin II induces LOX-1, the human endothelial receptor for oxidized low-density lipoprotein, Circulation 100 (1999) 899–902.
[40] W.S. Hummers Jr., R.E. Offeman, Preparation of graphitic oxide, J. Am. Chem. Soc. 80 (1958) 1339.
[41] S. Stankovich, D.A. Dikin, G.H. Dommett, K.M. Kohlhaas, E.J. Zimney, E.A. Stach, R.D. Piner, S.T. Nguyen, R.S. Ruoff, Graphene-based composite materials, Nature 442 (2006) 282–286.
[42] L. Michaelis, M.L. Menten, Die kinetik der invertinwirkung, Biochem. Z. 49 (1913) 352.
[43] T. Mosmann, Rapid colorimetric assay for cellular growth and survival: application to proliferation and cytotoxicity assays, J. Immunol. Methods 65 (1983) 55–63.
[44] O. Akhavan, E. Ghaderi, S. Aghayee, Y. Fereydooni, A. Talebi, The use of a glucose-reduced graphene oxide suspension for photothermal cancer therapy, J. Mater. Chem. 22 (2012) 13773–13781.
[45] D. Yang, A. Velamakanni, G. Bozoklu, S. Park, M. Stoller, R.D. Piner, S. Stankovich, I. Jung, D.A. Field, C.A. Ventrice, Chemical analysis of graphene oxide films after heat and chemical treatments by X-ray photoelectron and Micro-Raman spectroscopy, Carbon 47 (2009) 145–152.
[46] Y. Guo, L. Deng, J. Li, S. Guo, E. Wang, S. Dong, Hemin- graphene hybrid nanosheets with intrinsic peroxidase-like activity for label-free colorimetric detection of single-nucleotide polymorphism, ACS Nano 5 (2011) 1282–1290.
[47] Y. Qutub, V. Uzunova, O. Galkin, P.G. Vekilov, Interactions of hemin with model erythrocyte membranes, J. Phys. Chem. B 114 (2010) 4529–4535.
[48] B. Tian, C. Wang, S. Zhang, L. Feng, Z. Liu, Photothermally enhanced photodynamic therapy delivered by nano-graphene oxide, ACS Nano 5 (2011) 7000–7009.
[49] L. Jin, K. Yang, K. Yao, S. Zhang, H. Tao, S.-T. Lee, Z. Liu, R. Peng, Functionalized graphene oxide in enzyme engineering: a selective modulator for enzyme activity and thermostability, ACS Nano 6 (2012) 4864–4875.
[50] T. Eberlein, U. Bangert, R. Nair, R. Jones, M. Gass, A. Bleloch, K. Novoselov, A. Geim, P. Briddon, Plasmon spectroscopy of free-standing graphene films, Phys. Rev. B 77 (2008) 233406–233410.
[51] Z.H. Ni, T. Yu, Y.H. Lu, Y.Y. Wang, Y.P. Feng, Z.X. Shen, Uniaxial strain on graphene: Raman spectroscopy study and band-gap opening, ACS Nano 2 (2008) 2301–2305.
[52] C. Shan, H. Yang, D. Han, Q. Zhang, A. Ivaska, L. Niu, Graphene/AuNPs/chitosan nanocomposites film for glucose biosensing, Biosens. Bioelectron. 25 (2010) 1070–1074.
[53] C. Shan, H. Yang, D. Han, Q. Zhang, A. Ivaska, L. Niu, Electrochemical determination of NADH and ethanol based on ionic liquid-functionalized graphene, Biosens. Bioelectron. 25 (2010) 1504–1508.
[54] Y. Song, K. Qu, C. Zhao, J. Ren, X. Qu, Graphene oxide: intrinsic peroxidase catalytic activity and its application to glucose detection, Adv. Mater. 22 (2010) 2206–2210.
[55] Y.-l. Dong, H.-g. Zhang, Z.U. Rahman, L. Su, X.-j. Chen, J. Hu, X.-g. Chen, Graphene oxide-Fe_3O_4 magnetic nanocomposites with peroxidase-like activity for colorimetric detection of glucose, Nanoscale 4 (2012) 3969–3976.
[56] M. Ma, Y. Zhang, N. Gu, Peroxidase-like catalytic activity of cubic Pt nanocrystals, Colloids Surf. A: Physicochem. Eng. Aspects 373 (2011) 6–10.
[57] H. Zhang, X. Lv, Y. Li, Y. Wang, J. Li, P25-graphene composite as a high performance photocatalyst, ACS Nano 4 (2009) 380–386.
[58] I.V. Lightcap, T.H. Kosel, P.V. Kamat, Anchoring semiconductor and metal nanoparticles on a two-dimensional catalyst mat. Storing and shuttling electrons with reduced graphene oxide, Nano Lett. 10 (2010) 577–583.
[59] Z. Chen, S. Berciaud, C. Nuckolls, T.F. Heinz, L.E. Brus, Energy transfer from individual semiconductor nanocrystals to graphene, ACS Nano 4 (2010) 2964–2968.
[60] C.K. Duesterberg, S.E. Mylon, T.D. Waite, pH effects on iron-catalyzed oxidation using Fenton's reagent, Environ. Sci. Technol. 42 (2008) 8522–8527.
[61] H. Wei, E. Wang, Fe3O4 magnetic nanoparticles as peroxidase mimetics and their applications in H2O2 and glucose detection, Anal. Chem. 80 (2008) 2250–2254.
[62] E.S. Forzani, H. Zhang, L.A. Nagahara, I. Amlani, R. Tsui, N. Tao, A conducting polymer nanojunction sensor for glucose detection, Nano Lett. 4 (2004) 1785–1788.
[63] X. Yang, X. Zhang, Y. Ma, Y. Huang, Y. Wang, Y. Chen, Superparamagnetic graphene oxide-Fe_3O_4 nanoparticles hybrid for controlled targeted drug carriers, J. Mater. Chem. 19 (2009) 2710–2714.
[64] M.-T. Zhu, Y. Wang, W.-Y. Feng, B. Wang, M. Wang, H. Ouyang, Z.-F. Chai, Oxidative stress and apoptosis induced by iron oxide nanoparticles in cultured human umbilical endothelial cells, J. Nanosci. Nanotechnol. 10 (2010) 8584–8590.
[65] K. Yang, S. Zhang, G. Zhang, X. Sun, S.-T. Lee, Z. Liu, Graphene in mice: ultrahigh in vivo tumor uptake and efficient photothermal therapy, Nano Lett. 10 (2010) 3318–3323.
[66] C. Wang, L. Cheng, Z. Liu, Drug delivery with upconversion nanoparticles for multi-functional targeted cancer cell imaging and therapy, Biomaterials 32 (2011) 1110–1120.
[67] C. Xu, X. Wang, J. Zhu, Graphene- metal particle nanocomposites, J. Phys. Chem. C 112 (2008) 19841–19845.
[68] H. Ha, H.B. Lee, Reactive oxygen species as glucose signaling molecules in mesangial cells cultured under high glucose, Kidney Int. 58 (2000) S19–S25.
[69] W. Zhang, S.L. Hu, J.J. Yin, W.W. He, W. Lu, M. Ma, N. Gu, Y. Zhang, Prussian blue nanoparticles as multienzyme mimetics and reactive oxygen species scavengers, J. Am. Chem. Soc. 138 (2016) 5860–5865.
[70] F. Li, H. Yang, C. Shan, Q. Zhang, D. Han, A. Ivaska, L. Niu, The synthesis of perylene-coated graphene sheets decorated with Au nanoparticles and its electrocatalysis toward oxygen reduction, J. Mater. Chem. 19 (2009) 4022–4025.
[71] J. Wörle-Knirsch, K. Pulskamp, H. Krug, Oops they did it again! Carbon nanotubes hoax scientists in viability assays, Nano Lett. 6 (2006) 1261–1268.
[72] F. Perreault, A.F. de Faria, S. Nejati, M. Elimelech, Antimicrobial properties of graphene oxide nanosheets: why size matters, ACS Nano 9 (2015) 7226–7236.
[73] W. Xu, N. Mao, J. Zhang, Graphene: a platform for surface-enhanced raman spectroscopy, Small 9 (2013) 1206–1224.